Egyptian Journal of Radiology and Nuclear Medicine

RESEARCH

Open Access

Multi-phasic magnetic resonance imaging of hemodynamic interchanges in hepatocarcinogenesis

Ahmed Mahmoud Elzeneini[1], Mohsen Ahmed Abdelmohsen[2*] and Mohamed Ibrahim Yousef[3]

Abstract

Background Liver cirrhosis and hepatocellular cancer deem a substantial global health burden and are the end result of a variety of chronic liver diseases. Guidelines have been introduced to secure standardized approaches in the diagnosis and management of hepatocellular carcinoma (HCC). Established guidelines agree upon the distinctive dynamic enhancement findings of HCC, characterized by arterial phase wash-in and venous or delayed phase washout. The indeterminate focal hepatic lesions constitute a diagnostic dilemma. The aim of the study was quantification of hepatic vascular parameters using dynamic contrast-enhanced (DCE)-MRI to study liver hemodynamic disturbances that can differentiate between focal hepatic lesions during hepatocellular carcinogenesis.

Results The study was conducted on 95 patients with comparing perfusion abnormalities across different liver cirrhosis pathologies, and the comparison revealed the correlation of hemodynamics with hepatocarcinogenesis and grades of cirrhosis. Relative enhancement curves were graphed to illustrate the different enhancement patterns across the spectrum of hepatonodular lesions of cirrhosis and among types of de novo and recurrent HCC. Statistical significance was highest between dysplastic nodules (DNs) and HCCs (maximal relative enhancement (MRE) 0.88, wash-in ratio (WIR) 0.84, washout ratio (WOR) 0.78, time to peak (TTP) 0.74, area under curve (AUC 0.73, T_0 0.70), compared to those between cirrhotic liver and DNs (MRE 0.74, To 0.62). Least significances were between de novo and recurrent HCCs (TTP 0.66, r AUC 0.66, MRE 0.63). Performances between non-cirrhotic and cirrhotic liver [WOR 0.81, time to peak (TTP) 0.80, r AUC 0.63] surpassed those among different grades of cirrhosis (the highest was between non-tumoral and tumoral cirrhosis: TTP 0.74, MRE 0.68, WIR 0.65, WOR 0.65).

Conclusions Dynamic contrast-enhanced magnetic resonance imaging hemodynamic metrics promise potential usefulness as non-invasive biomarkers in assessment of liver cirrhosis, characterization of cirrhotic nodules, and evaluation of multistep hepatocarcinogenesis.

Keywords Liver cirrhosis, Dysplastic nodule, HCC, DCE-MRI, Semiquantitative analysis

*Correspondence:
Mohsen Ahmed Abdelmohsen
Mohsenmohsenmd@yahoo.com
Full list of author information is available at the end of the article

Background

The liver orchestrates metabolism in the human body and regulates a multitude of essential physiological processes [1]. Liver cirrhosis and hepatocellular cancer are the end result of a variety of chronic liver diseases, including viral hepatitis, alcohol/aflatoxin-induced liver disease, and non-alcoholic steatohepatitis [2].

Liver cirrhosis is characterized by hepatic fibrosis, altered extracellular composition, and increased vascular bed resistance [3]. These changes contribute to the deteriorated hepatic function by compromising transsinusoidal blood hepatocyte exchange and altering liver hemodynamics [4]. The quantification of hepatic vascular parameters using dynamic contrast-enhanced (DCE) MRI has the potential to study liver hemodynamic disturbances [5, 6] that underpin the pathophysiology of chronic liver disease [7, 8].

Surveillance and early detection of HCC is crucial for curative resection, liver transplantation, and effective intervention [9].

Established guidelines agree upon the distinctive dynamic enhancement findings of HCC, characterized by arterial phase wash-in and venous or delayed phase washout [10].

The American Association for the Study of Liver Diseases (AASLD), the European Association for the Study of the Liver (EASL), and Liver Imaging Reporting and Data System (LIRADS) guidelines endorse dynamic cross-sectional imaging [9] with the use of extracellular contrast [10] to assess worrisome, 1cm or larger, nodules. In addition, the modified Response Evaluation Criteria in Solid Tumors (mRECIST) advocates the use of percentage change in residual lesion enhancement for treatment response assessment [9, 11].

Research is focused on functional imaging and the emergence of non-invasive biomarkers that can reliably reflect the changes in various tumoral microstructural [12–14] and microcirculatory parameters [15].

Sequential intranodular hemodynamic changes are concomitant with the multistep process of hepatocarcinogenesis [16], which entails the gradual dedifferentiation of cirrhotic to dysplastic nodule, followed by the evolution of HCC [17]. Intranodular arterial inflow increases and intranodular portal supply decreases as the disease advances [18, 19].

The evolution toward HCC is characterized by neovascular arterialization and sinusoidal capillarization [20]. Tumoral microvasculature is characterized by abnormal microvascular density and primitive hyperpermeable endothelial nature [21, 22].

Quantification of multiphase DCE-MRI signal change as a function of time is conducted to study perfusion changes [23, 24]. Semiquantitative analysis is a model-free approach that applies time–signal enhancement curves to derive physiologically interpretable and easily reproducible vascular measures [25]. On the other hand, quantitative analysis is a complex model-based approach that constructs pharmacokinetic modeling to reflect underlying physiological properties of studied tissue [26].

Dynamic contrast-enhanced magnetic resonance (DCE-MR) functional imaging and perfusion analysis of hepatic and tumoral vascular parameters promise potential usefulness in the assessment of liver cirrhosis and hepatocarcinogenesis [27].

Aim of the work

The aim was to evaluate the functional role of DCE-MRI analysis of perfusion changes in multistep hepatocarcinogenesis.

Methods

Patients

The study was designed to enroll two main groups of patients, namely cirrhotic and non-cirrhotic liver. The cirrhotic group included 53 patients, 36 males and 17 females, and their ages ranged from 42 to 73 years. On the other hand, the non-cirrhotic group included 42 patients, 15 males and 27 females, and their ages ranged from 36 to 55 years.

The patients were referred to the Radiology Department over a period of 24 months from January 2021 to January 2023.

All enrolled cirrhotic patients had chronic viral-related hepatitis with cirrhotic morphological changes, including those who had additional intrahepatic de novo or post-therapeutic recurrent lesions.

Conversely, all non-cirrhotic patients either tested negative for viral hepatitis or tested positive but had no evidence of cirrhotic morphological changes on conventional MRI and complementary ultrasound (US).

Written informed consent was obtained from all individual participants included in the study, which was approved by the institutional review board.

Study design This was a prospective cross-sectional study.

Inclusion criteria

1- Patients with CT indeterminate focal hepatic lesions.
2- Cirrhotic liver.
3- Positive virology profile.
4- Abnormal liver functions.

Exclusion criteria

1- General contraindications for MRI study: claustrophobia, pacemakers insertion, cochlear implants.
2- Estimated glomerular filtration rate less than 30.

MRI imaging

Magnetic resonance imaging (MRI) was conducted on a 3.0-T MR scanner (Philips Achieva, Philips Medical Systems, Netherlands) equipped with a phased-array torso surface coil.

Conventional MRI

Conventional unenhanced MRI sequences were obtained in axial plane utilizing respiratory-triggered techniques, with the following parameters:

- T1-weighted imaging (T1WI) including in-phase and opposed phase: (TR/TE = 10/4.6 ms, flip angle = 15°, section thickness = 7 mm, intersection gap = 2 mm, FOV = 300–350 mm).
- T2-weighted imaging (T2 WI): (TR/TE = 1000/80 ms, flip angle = 90°, section thickness = 7 mm, intersection gap = 2 mm, FOV = 300–350 mm).
- T2 fat-suppression (SPAIR): (TR/TE = 1000/80 ms, flip angle = 90°, section thickness = 7 mm, intersection gap = 2 mm, FOV = 300–350 mm).
- Diffusion-weighted imaging (DWI) including *b* values of 0, 200, 1000: (TR/TE = 1700/76 ms, section thickness = 7 mm, intersection gap = 2 mm, FOV = 300–350 mm).

Dynamic contrast-enhanced MRI

Dynamic MR imaging was then performed in axial plane utilizing breath-hold techniques. A series of 30 fat-suppressed T1-weighted spoiled gradient-echo sequences (THRIVE) were acquired using the following parameters: TR/TE = 4.6/2.3 ms, flip angle = 15°, breath-hold = 20 s, number of slices = 130–140, section thickness = 3 mm, intersection gap = 1.5 mm, FOV = 300–350 mm, and matrix size = 172 × 163.

An unenhanced dataset was first acquired prior to contrast administration. Intravenous bolus injection of 0.1 mmol/kg body weight of gadolinium-DTPA (Magnevist; Schering, Berlin, Germany) was administered at a rate of 2 ml/sec using an automatic injector, which provided the estimated glomerular filtration rate more than 30.

Four successive imaging datasets were acquired. Dynamic datasets were timed to start after the arrival of the contrast bolus to the aortic arch, according to the following: arterial phase 20–30 s, portal phase 50–60 s, late portal/venous phase 80–90 s, and delayed phase 150–180 s.

Automated digital subtracted images were generated, by subtraction of the pre-enhancement T1-THRIVE dataset from the corresponding multiphase series of post-enhancement datasets, together with color-scaled maps.

Standard of reference

It was unfeasible to attain pathological confirmation for all studied pathologies, as many of the patients were unfit for surgery. Moreover, biopsy is considered invasive and resulted in sampling errors when intended for small nodular lesions [28], as was the case for many of the lesions in our study. Hence, we designed our study according to the following detailed standards of reference.

Cirrhotic liver was either biopsy-proven (with or without additional hepatocellular pathology), or confirmed by radiologically evident cirrhotic morphology on conventional MR imaging and complementary US. *"The cirrhotic liver develops characteristic morphological alterations such as surface nodularity, widening of fissures, expansion of the gallbladder fossa, notching of the right lobe, atrophy of the right lobe, and relative enlargement of the left lobe and caudate lobe"* according to Faria et al. [29].

Non-cirrhotic liver was confirmed radiologically by the absence of any cirrhotic morphological changes on conventional MRI and complementary US. Non-cirrhotic patients were tested for virology and categorized accordingly.

De novo and *recurrent HCC* was either biopsy-proven or radiologically diagnosed by characteristic HCC enhancement criteria on dynamic MRI best appreciated on subtracted images [30–32] according to LIRADS, AASLD, and EASL.

Indeterminate dysplastic nodule category included both of the following: *"high-grade dysplastic nodules"* and the grossly indistinguishable *"early, vaguely nodular, hypovascular HCCs with indistinct margins,"* whereby both range 1–1.5 cm and *"usually have similar diminished arterial and portal venous flow and hence are both hypoenhanced relative to the background liver in arterial and portal venous phases"* [20].

Peri-ablation hyperemic rim referred to benign hyperemic ring-like enhancement that persisted on delayed phases, according to Luo et al. [33].

Tumor in vein (TIV) included thrombus involvement of the PV with detectable tumor enhancement on post-contrast dynamic series [34].

Imaging analysis

The review of all conventional and dynamic MR imaging was performed on the 3-T MR Unit workstation, utilizing the commercially available software (Philips Medical Systems), by two of the authors, a clinical radiologist with 5 years of experience and another clinical radiologist with 7 years of experience in cross-sectional MR imaging with 100% inter-observer agreement.

Conventional MR images were thoroughly assessed, and lesions were located and characterized according to their number, size, shape, signal criteria, and restriction pattern. Dynamic series with color maps and subtraction datasets were analyzed for lesion enhancement patterns and heterogeneity. In lesions with heterogeneous enhancement, areas of max hypervascularity were identified. Inherent/post-ablation precontrast T1 hyperintensities were subtracted out, and the presence of hypervascularity was confirmed.

Three user-defined regions of interest (ROIs) were placed on areas of maximum hyper vascularity in each of the identified lesions. Three ROIs were also randomly placed in the lesion-free or lesion-bordering liver parenchyma in each patient, together with one ROI in the descending abdominal aorta, PV, and IVC. ROIs were standardized 2.1 mm^2.

The direct use of time–signal changes would lead to inaccurate quantitation of enhancement owing to the differences in inherent T1 signal properties of studied tissues [35]. Time–signal intensity curves were normalized to baseline signals to reconstruct time-relative enhancement curves (RE-T). From these curves, a variety of hemodynamic metrics can then be derived.

Maximum relative enhancement (MRE), area under the curve (AUC), wash-in ratio (WIR), washout ratio (WOR), time to arrival (TOA), and time to peak (TTP) measurements were automatically generated, averaged, and tabulated.

In addition, the relative area under the curve (r AUC) was manually calculated, averaged, and then tabulated, for each of the above pre-defined ROIs.

Statistical analysis

All data were expressed as mean ± standard deviation. Unpaired Student t tests were used to compare different, normally distributed, hemodynamic parameters between the different lesion groups as well as between the different cirrhotic grades. Welch's correction was used to correct for statistically significant unequal variances.

Data analyses were performed on a personal computer using: *GraphPad Prism version 6.00 for Windows, GraphPad Software, La Jolla, California, USA.*

Receiver operating characteristic (ROC) curve was constructed, and the diagnostic performances were extracted by measurements of the area under the ROC curves. Postulated cut-off values were presented with their specificities and sensitivities. Mean time–%relative enhancements were graphed.

Results

The non-cirrhotic group was divided into *"normal liver with positive virology"* (30 patients) and *"normal liver with negative virology"* (12 patients). On the other hand, the cirrhotic group was divided into *"stand-alone liver cirrhosis"* (10 patients) and *"liver cirrhosis with pathological lesions"* (43 patients with 87 different lesions) (Fig. 1).

The liver cirrhosis with pathological lesion group was further divided according to the nature of the lesion (14 DNs, 52 de novo HCCs, 16 recurrent HCCs, 2 malignant PV thrombi, and 3 peri-ablation hyperemic rims).

The 52 de novo HCCs were subcategorized into 45% nodular HCC, 34% large HCC, and 21% capsulated HCC (nodular HCC < 2 cm, distinctly nodular or discretely multinodular (Fig. 2a), moderately differentiated, progressed HCC; large HCC > 2 cm, pseudo-encapsulated (Fig. 2c) or locally infiltrative (Fig. 2e), poorly differentiated, progressed HCC; and capsulated HCC > 2 cm, and true fibrous capsulated (Fig. 3)).

But the 16 recurrent HCCs were subcategorized into 68% nodular recurrence and 32% large recurrence (nodular recurrence < 2 cm, distinctly nodular or discretely multinodular recurrent HCC (Fig. 4), and large recurrence > 2 cm, encapsulated or locally infiltrative recurrent HCC (Fig. 5)).

The 43 cirrhotic livers with pathological lesion/s were composed of 67% *"liver cirrhosis harboring HCC"* and 33% *"liver cirrhosis harboring dysplastic nodule."*

Data analyses were tabulated as mean ± standard deviation (Table 1).

Semiquantitative DCE-MRI parameters in hepatocarcinogenesis

Statistical interrogation comparing different perfusion metrics across different hepatocellular lesions of cirrhosis revealed the correlation of intranodular hemodynamics with multistep hepatocarcinogenesis (Fig. 6).

Statistically significant performances were highest between DNs and HCCs intranodular hemodynamics (diagnostic accuracies: MRE 0.88, WIR 0.84, WOR 0.78, TTP 0.74, AUC 0.73, T_0 0.70), compared to those between cirrhotic liver and DNs (diagnostic accuracies: MRE 0.74, T_0 0.62) (Table 2).

Statistical performance was least significant between de novo and recurrent HCCs (diagnostic accuracies: TTP 0.66, r AUC 0.66, MRE 0.63) (Table 2).

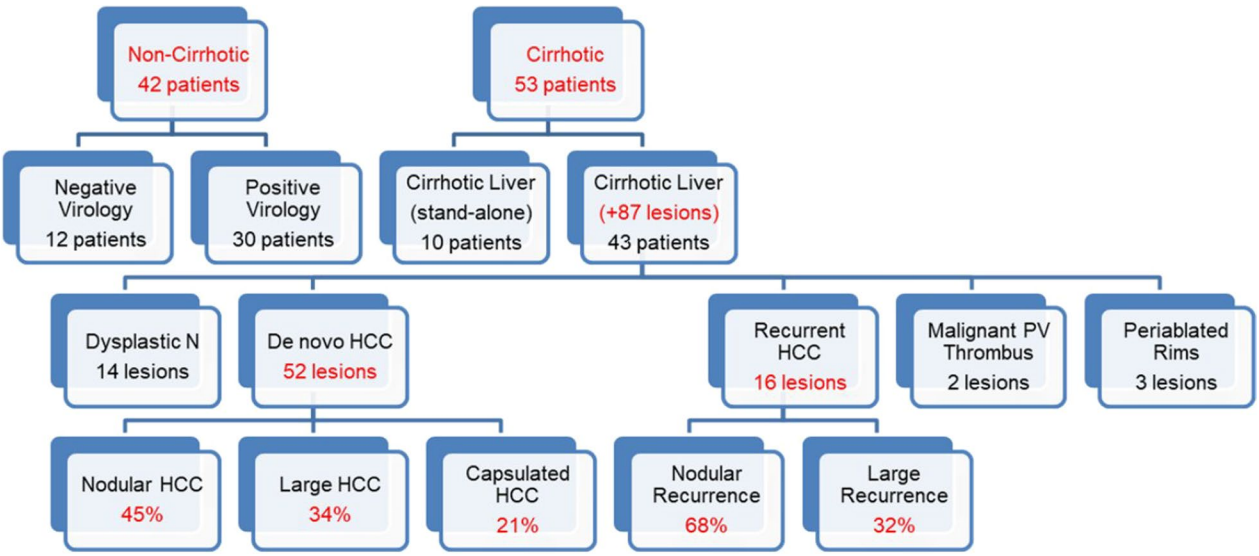

Fig. 1 Schematic diagram outlining the design of the study

Mean time–%relative enhancement curves were graphed to illustrate the different enhancement patterns across the spectrum of hepatonodular lesions of cirrhosis (Fig. 7) and among types of de novo and recurrent HCC (Fig. 8).

Discussion

Dynamic contrast-enhanced MRI functional imaging is primarily focused on quantitative evaluation of tumoral perfusion and permeability as opposed to conventional MR structural imaging that focuses on the qualitative assessment of tumoral morphology and degree of enhancement, thus enabling an insight into the pathophysiology of tissue [36]. Physiologic changes that precede morphological changes serve as early biological markers of tumorigenesis and response to treatment [37].

The aim of our study was to evaluate the functional role of DCE-MRI analysis of perfusion changes in multistep hepatocarcinogenesis.

Perfusion in the microcirculation, estimated by semi-quantitative first-pass metrics such as WIR and MRE [38, 39], and accumulation in the interstitium, measured by quantitative parameters such as $K^{-1\,0}$ (leakage into interstitium) and K-ep (return from interstitium to plasma), are two discrete successive phenomena that overlap [40]. Despite the complexity of pharmacokinetic models, it has been proposed that simple relative enhancement curves are equally representative [35], whereby post-peak and late enhancement phases can simulate K^{-trans} and K-ep, respectively [40].

The hepatocarcinogenic spectrum from benign regenerative to premalignant dysplastic nodules, followed by carcinogenesis of early vaguely nodular HCC, and progression to less differentiated HCC involves a sequential alteration in intranodular hemodynamics [41].

Understanding the interchanging dynamics of hepatonodular inflows and outflows is essential to correlate imaging criteria with histopathology [19]. Interestingly enough, we managed to mirror this sequential interchange in hepatonodular flow kinetics and illustrate the different multiphase enhancement patterns across the carcinogenic continuum. The nodular phenotype is determined through angiogenic activity and interchange in drainage channels [36]. Angiogenesis, provoked by tissue hypoxia and vascular endothelial growth factors (VEGF) [35], is essential for tumor initiation. Concurrent interchange in drainage vessels is characteristic for tumor progression [42].

Regarding hepatonodular inflows: Considerable overlap in radiological criteria occurs between high-grade dysplastic nodules and early hypo vascular HCC. Both are similarly hypovascular to background liver [41] as demonstrated on perfusion-weighted MRI by Elzenine et al. [23], due to their impaired native portal flow and insufficient pathological unpaired arterial growth [16]. The only distinguishing feature, namely stromal invasion, can even be missed by histopathology [43]. Having said that, it is crucial to point out that high-grade dysplastic nodules are considered premalignant and reported to transform into early HCC in periods as short as 4-month duration [11].

The current study results revealed outstanding diagnostic performance across all hemodynamic metrics when comparing this premalignant indeterminate

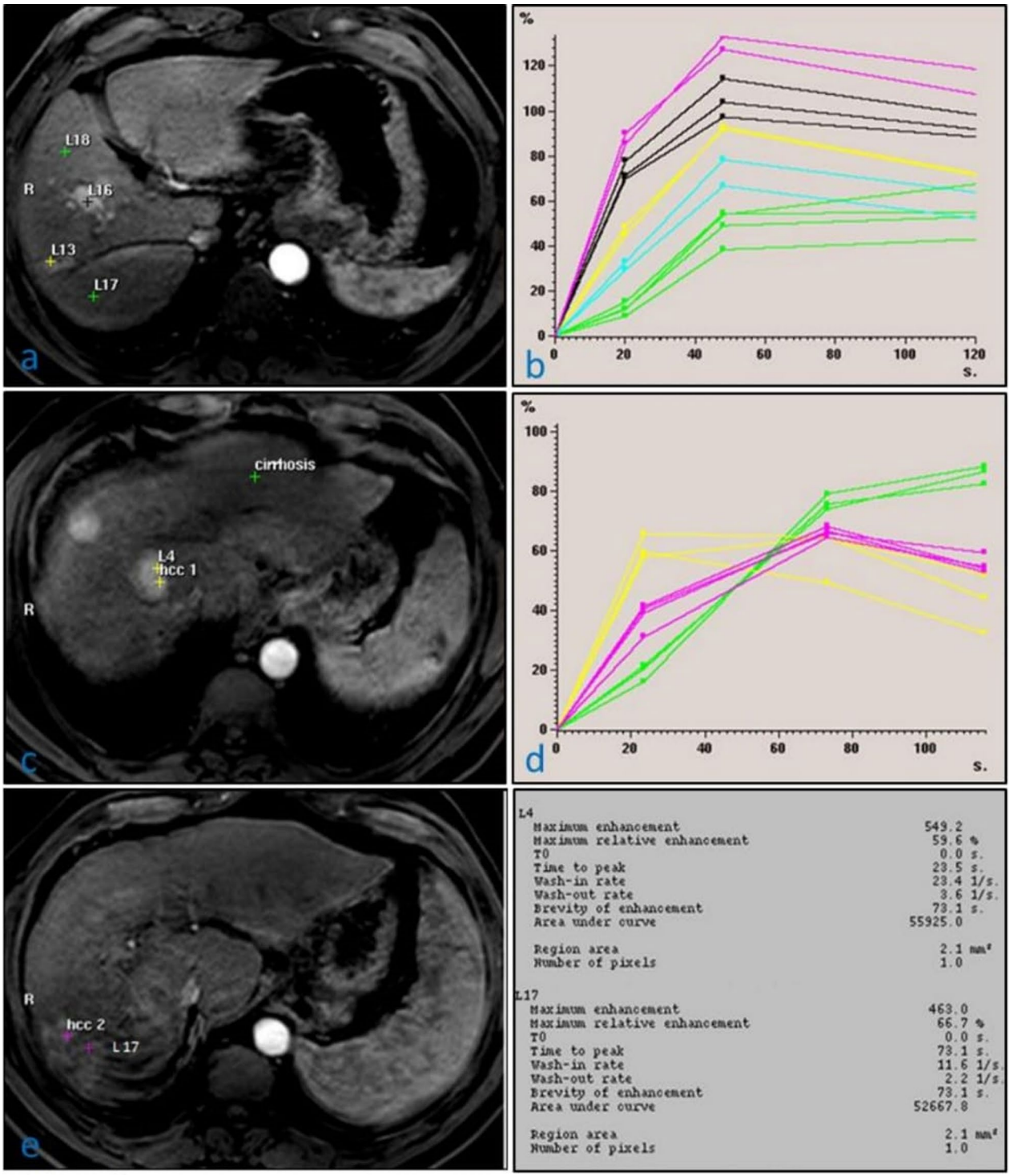

Fig. 2 A 45-year-old male patient presented with liver impairment, jaundice liver cirrhosis: **a** Liver cirrhosis with multifocal multinodular de novo HCCs on arterial phase MRI; **b** corresponding time–%relative enhancement curves of the different nodular HCC grades (colors) and adjacent lesion-free cirrhosis (green) are shown. **c** and **e** Liver cirrhosis presented with multicentric large HCCs: pseudo-encapsulated (Hcc 1) and locally invasive (Hcc 2) subtypes on arterial phase MRI; **d** corresponding time–%relative enhancement curves of the lesion-free cirrhosis (green) and different large HCC subtypes (yellow) and (purple), with their hemodynamic metrics (L4) and (L17), respectively

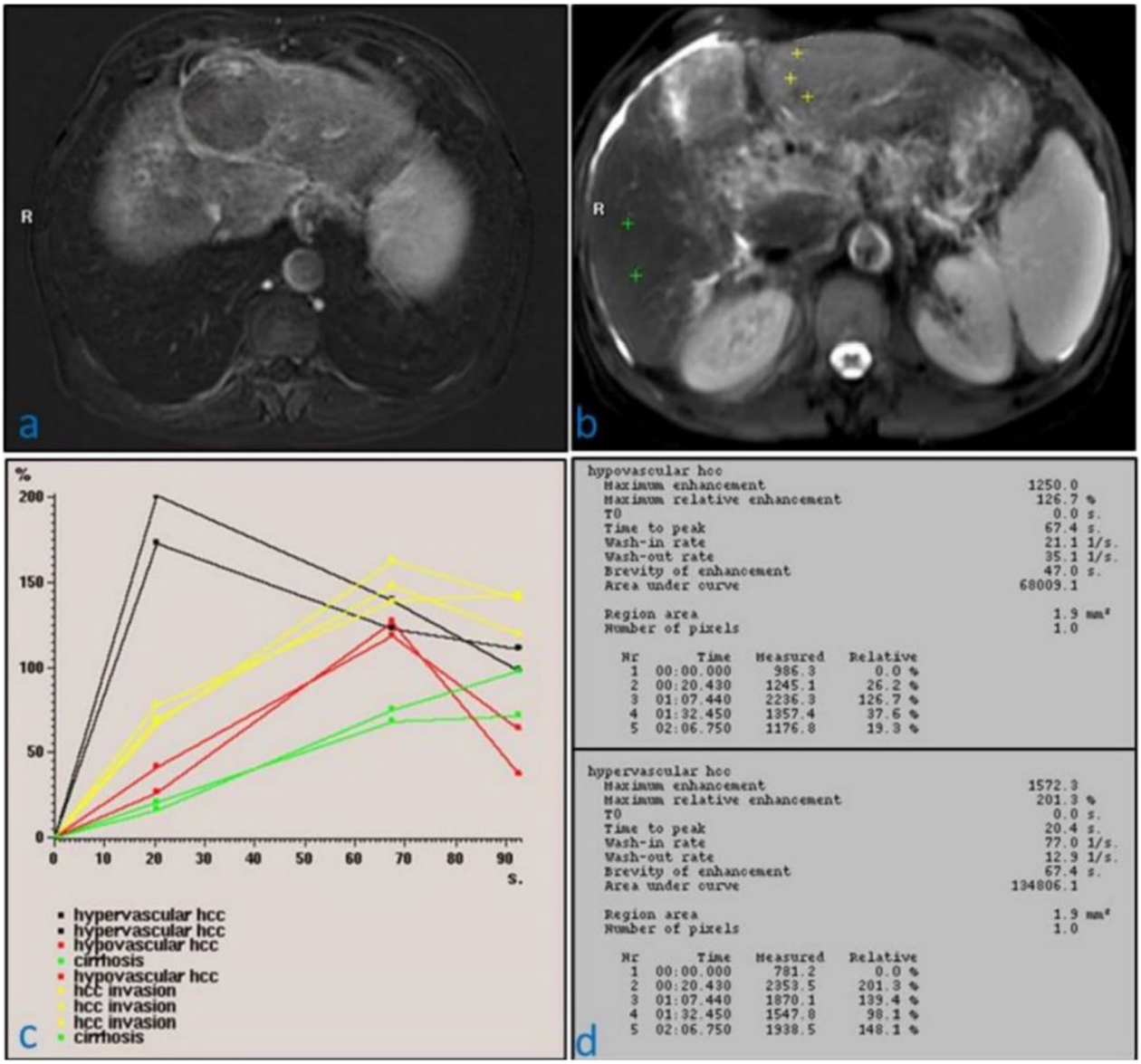

Fig. 3 A 53-year-old female patient presented with liver cirrhosis, CT-detected indeterminate focal hepatic lesion **a** liver cirrhosis with a large true fibrous capsulated HCC that reveals tumoral enhancement heterogeneity on late phase MRI; **b** together with subsequent underlying hepatic parenchymal invasion depicted on T2 fat-suppressed WI; **c** corresponding time–%relative enhancement curves of the hypovascular (red) and hypervascular (black) tumoral enhancement, as well as the underlying hepatic parenchymal invasion (yellow) and lesion-free cirrhosis (green) are shown; **d** hemodynamic metrics of hypovascular and hypervascular tumoral regions

category (nodule D) with established carcinogenesis (HCC N).

Tissue perfusion and microvascular density indicators, namely MRE and WIR, surpassed the remaining hemodynamic metrics in performance. Intranodular MRE exceeding 83%, reflecting both intra- and extravascular first-pass kinetics [44], provided the foremost reliable differentiation of nodular HCC from premalignant nodules with 88% accuracy and up to 94% confidence. Intranodular WIR more than 18 Usec, reflecting exclusive intravascular first-pass kinetics [44], ranked second with 84% accuracy and up to 92% confidence. This precedence of MRE over WIR could be attributed to the added effect of the tumoral microvascular blood volume that is more accounted for using maximum enhancement than first-pass increment [45].

Many researchers had comparably presented a variety of first-pass perfusion metrics such as WIR and first-pass

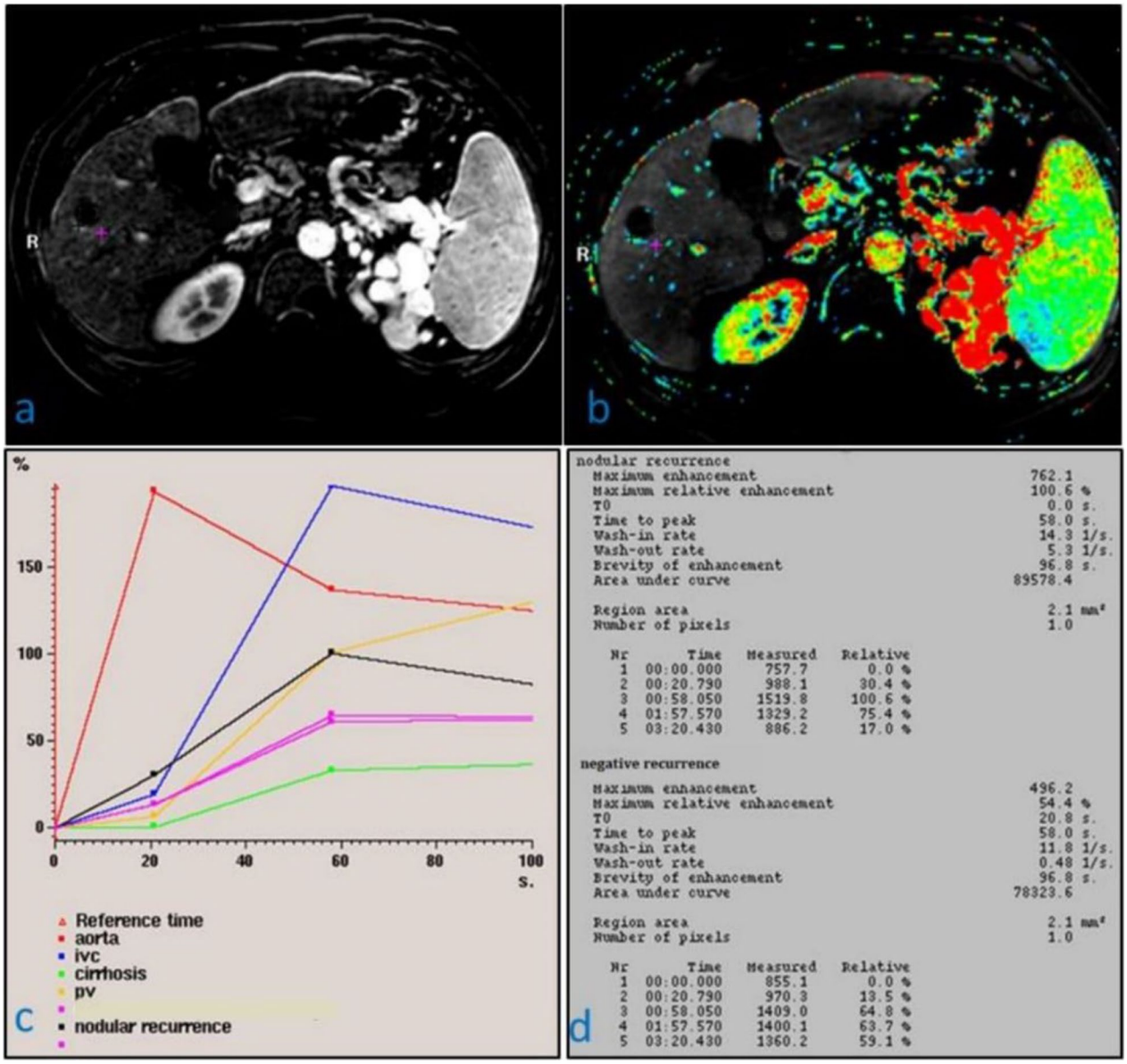

Fig. 4 A 56-year-old male patient presented with HCC lesion managed by radiofrequency ablation with suspected recurrence: **a** liver cirrhosis with previously ablated hepatic focal lesion currently presented with tiny focal enhancement worrisome for focal nodular outgrowth recurrence on digital subtraction arterial phase MRI; **b** corresponding color-scale relative enhancement mapping MRI allows enhanced identification of the nodular focus of maximum relative enhancement; **c** corresponding time–% relative enhancement curves of the aorta (red), PV (dark yellow), IVC (blue), lesion-free cirrhosis (green), adjacent perilesional hyperemia negative for recurrence (purple), and focal tiny nodular hyperenhancement with characteristic wash-in and washout positive for early nodular outgrowth recurrence (black); **d** quantitative comparison of the hemodynamic metrics of negative versus positive early nodular tumoral recurrence

RE by Wang et al. [46], RAE by Ippolito et al. [47], MRE by Elzenini et al. [23], and first-pass initial AUC by Zhang et al. [15].

They all performed as reasonable indicators for tumoral perfusion [48].

The timing of the intranodular contrast increment (T Peak) less than 55.5 s (74% accuracy) outperformed that of contrast arrival (T Zero) less than 7 s (70% accuracy), when used to signal out carcinogenesis. We accounted the under-performance of T Zero to the effect of physiological body functions on the rate of contrast delivery to the tissue, such as cardiac function [23]. In our study, AUG ranked late in diagnosing HCC with 73% accuracy, as opposed to better performing first-pass initial AUC,

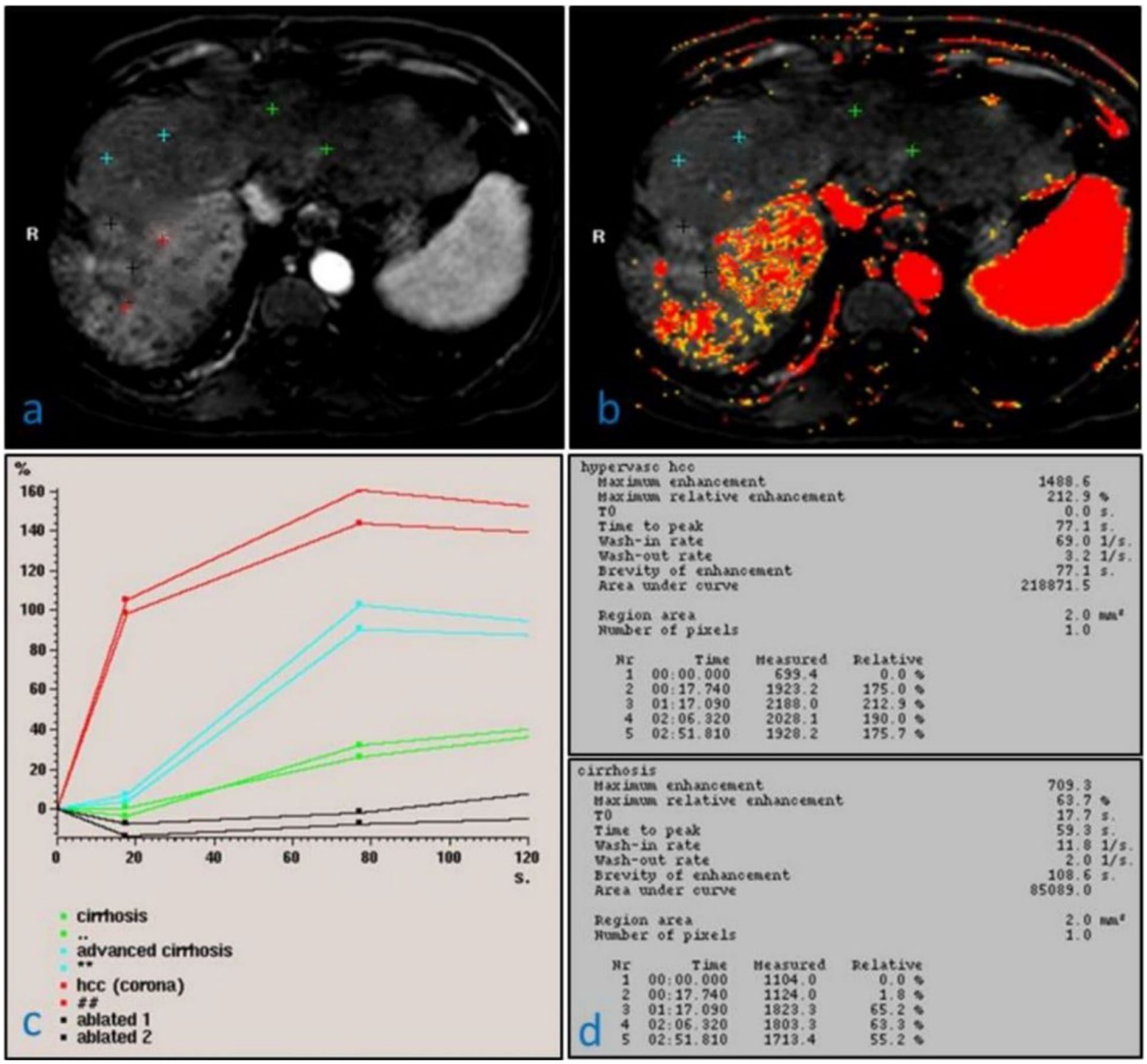

Fig. 5 A 62-year-old male patient presented with liver cirrhosis and HCC lesion managed by radiofrequency ablation with suspected recurrence: **a** advanced liver cirrhosis with recently ablated two adjacent hepatic focal lesions [black plus (**+**) symbols] as evidenced by the signs of intra-lesional coagulative necrosis and right subcapsular juxta-lesional RF needle track, currently presented on follow-up imaging with massive infiltrative territory of heterogeneous hyperenhancement [red plus (+) symbol] on arterial phase MRI; **b** corresponding color-scale relative enhancement mapped MRI further enhances the intensity and heterogeneity of this infiltrative tumoral hyperenhancement; **c** and **d** corresponding time–%relative enhancement curves and quantitative hemodynamic metrics compare the non-viable ablated lesions (black) versus the surrounding massive infiltrative readily washed out hyperenhancement positive for viable large recurrence (red), and compare as well the nearby right lobe advanced cirrhotic background (turquoise) versus the contralateral left lobe relatively less advanced cirrhosis (green)

used by other researchers as Zhang et al. [15]. Moreover, our results undermined the significance of relative AUC, a relative metric proposed by Cuenod and Balvay [21], when utilized as a marker of carcinogenesis.

Regarding hepatonodular outflows: Kitao et al. [42] explained that invasion of the intranodular hepatic veins first occurs through carcinogenic replacement growth, because of the absence of perivascular connective tissue covering. Collapse of intra- and peri-nodular hepatic sinusoid drainage then follows by tumorigenic compressive growth. Reversed portal venous outflow and subsequent extension of peritumoral corona enhancement finally proceed in line with tumor progression [16]. These interchanging outflow dynamics have been well reflected

Table 1 Hepatocarcinogenesis hemodynamics (mean ± SD)

Data	MRE		WIR		WOR		AUC		r AUC		*T* Zero		*T* Peak	
	Mean	SD	Mean	SD	Mean	SD	Mean	SD	Mean	SD	Mean	SD	Mean	SD
Liver N	77.8	18.8	20.4	8.6	3.2	2.0	109.3	64.0	22.6	5.5	17.1	8.0	52.9	17.4
Liver C	80.0	24.3	16.7	8.1	1.1	1.3	94.8	54.3	26.8	9.4	20.3	13.5	94	47.5
Nodule D	59.9	20.5	15.5	7.4	1.6	1.3	79.4	41.2	33.7	18.9	14.1	15.2	80.4	38.4
HCCN	109.7	38.0	34.7	22.4	5.1	6.3	131.3	71.3	36.9	13.6	4.3	11.2	52.0	24.3
HCCR	126.3	36.9	34.2	16.6	4.8	3.1	155.0	80.7	44.4	116	2.9	8.7	64.4	18.6
pv T	129.1	26.8	30.8	5.0	3.9	4.2	146.1	38.5	37.3	6.4	8.3	7.8	111.1	101.2
Ablated *R*	174.9	48.1	24.4	8.3	2.2	2.2	152	47.7	38.6	6.6	0	0	78.6	4.0

Liver N Non-cirrhotic liver, *Liver C* Cirrhotic liver, *Nodule D* Indeterminate dysplastic nodule, *HCC N* De novo HCC, *HCC R* Recurrent HCC, *Ablated R* Recurrence after ablation, *MRE* Maximum relative enhancement, *WIR* Wash-in ratio, *WOR* Washout ratio, *T Peak* Time to peak, *T Zero* Time to arrival, *AUC* Area under the curve

in our multiphase enhancement patterns evidenced by the transition from weak late venous washout in indeterminate dysplastic nodules to strong early portal washout in nodular carcinogenesis. Furthermore, we propose that quantitated intranodular WOR, exceeding 2.2 Lisee, could be implemented as a biomarker for HCC with a reasonable accuracy of 78%.

Progression of hepatocarcinogenesis involves concurrent changes in tumoral tissue microvascular architecture (density) and properties (permeability) [41]. We attempted to simulate this altered microvascular environment through mirroring the different enhancement patterns across different tumoral grades. We reported that less differentiated and more progressed large HCCs tend to generally express higher first-pass RAE, shallower wash-in, and weaker washout as opposed to the more differentiated and less progressed small HCC. These results were contradicted the Yamashita et al. [49] study.

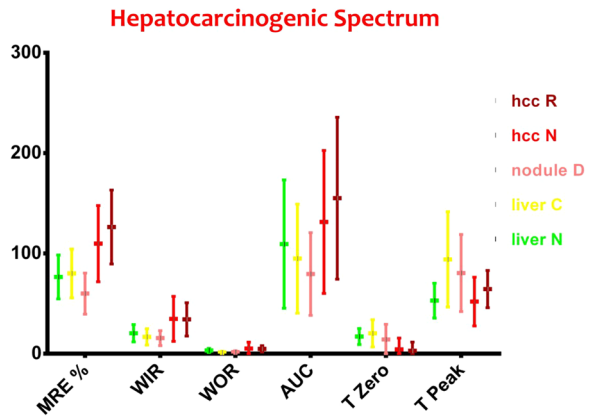

Fig. 6 Illustrative graph showing the interchanging intranodular hemodynamics across the spectrum of hepatocellular carcinogenesis. *Note* non-cirrhotic liver (liver N), cirrhotic liver (liver C), indeterminate dysplastic nodule (nodule D), de novo HCC (HCC N), recurrent HCC (HCC R), maximum relative enhancement (MRE), wash-in ratio (WIR), washout ratio (WOR), time to peak (T Peak), time to arrival (T Zero), area under the curve (AUC)

Differences in poorly differentiated HCC enhancement kinetics could be explained by the more limited tumoral vascular reserve [44] because of reduced microvascular density [13] and the increased extracellular space [23]. Moreover, large fibrous capsulated, more progressed HCC [32] presented higher first-pass RAE, steeper washin, and stronger washout with characteristic corona enhancement as opposed to small nodular, less progressed HCC. Corona enhancement was the initial site of drainage [50] and recurrence. Quantitated MRE and T Peak underperformed in differentiating recurrent from de novo HCC.

Furthermore, therapeutic evaluation can be reliably monitored by DCE-MR. Several studies assessing treatment response, such as Wang et al. [46] expressed significant differences in hemodynamic parameters, namely MRE and AUC, respectively, between anti-angiogenic responders and non-responders [27]. Hence, future trends in research advocate the use of DCE -MR imaging in the assessment of targeted HCC therapy [8].

Likewise, the *continuum of hepatofibrogenesis* is accompanied by gradual obliteration of normal vascular and sinusoidal channels, thus increasing the vascular bed resistance [5], slowing the blood passage through the parenchyma, and altering the liver hemodynamics [29].

In our study, TTP excelled in diagnostic performance as a non-invasive early biological surrogate to differentiate between cirrhotic and non-cirrhotic liver scoring 80% accuracy, DO RKG et al. [27], had also previously confirmed, by histology, that mean transit time (MTT) was most sensitive and specific for assessing the severity of fibrosis.

Finally, the uniqueness of our study resides in its attempt to shed light on diagnostic capacity of perfusion MRI using both "relative enhancement curveology" and "semiquantitative perfusion analyses."

Liver Imaging Reporting and Data System (LIRADS) was applied since 2013, and the LIRADS categories

Table 2 Hepatocarcinogenesis hemodynamics (diagnostic performances)

Data	Significance	ROC	95% CI	Cut off	Sensitivity	Specificity
Liver C versus liver N						
WOR	****	0.81	0.75–0.87	< 1.25 L/s	0.67	0.82
T Peak	****	0.80	0.73–0.86	> 63 s	0.67	0.76
r AUC	**	0.63	0.55–0.72	> 25%	0.60	0.67
Nodule D versus liver C						
MRE	****	0.74	0.64–0.84	< 56%	0.59	0.82
T Zero	*	0.62	0.49–0.76	< 14 s	0.52	0.80
HCC N versus nodule D						
MRE	****	0.88	0.82–0.94	> 83%	0.74	0.82
WIR	****	0.84	0.76–0.92	> 18 L/s	0.78	0.75
WOR	****	0.78	0.69–0.77	> 2.2 L/s	0.68	0.70
T Peak	***	0.74	0.64–0.84	< 55.5 s	0.55	0.85
AUC	****	0.73	0.63–0.83	> 79.5 L/100 ml	0.77	0.59
T Zero	**	0.70	0.58–0.82	< 7 s	0.83	0.56
HCC R versus HCC N						
r AUC	**	0.66	0.56–0.75	> 47%	0.50	0.80
T Peak	**	0.66	0.57–0.76	> 65 s	0.53	0.78
MRE	*	0.63	0.54–0.72	> 115%	0.50	0.62

More asterisk indicate the more significance

Liver N Non-cirrhotic liver, *Liver C* Cirrhotic liver, *Nodule D* Indeterminate dysplastic nodule, *HCC N* De novo HCC, *HCC R* Recurrent HCC, *Ablated R* Recurrence after ablation, *MRE* Maximum relative enhancement, *WIR* Wash-in ratio, *WOR* Washout ratio, *T Peak* Time to peak, *T Zero* Time to arrival, *AUC* Area under the curve

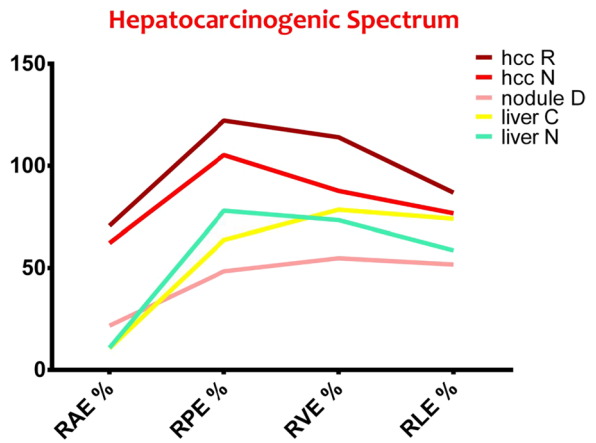

Fig. 7 Illustrative time–% relative enhancement graph showing the interchanging relative multiphase enhancement patterns across the different constituents of the spectrum of hepatocellular carcinogenesis. *Note* non-cirrhotic liver (liver N), cirrhotic liver (liver C), indeterminate dysplastic nodule (nodule D), de novo HCC (HCC N), recurrent HCC (HCC R), relative arterial enhancement (RAE), relative portal enhancement (RPE), relative venous enhancement (RVE), relative late enhancement (RLE)

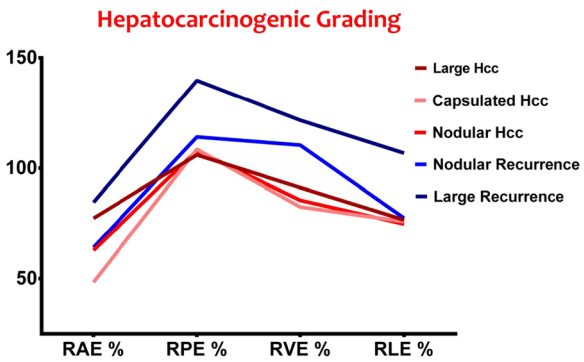

Fig. 8 Illustrative time–%relative enhancement graph comparing the varying relative multiphase enhancement patterns across the different de novo HCC subtypes and recurrent HCC grades. *Note* relative arterial enhancement (RAE), relative portal enhancement (RPE), relative venous enhancement (RVE), relative late enhancement (RLE)

reflect probabilities; they do not correspond to exact histological categories [51, 52]. The observations noted such as regenerating and dysplastic nodules are categorized LR2 (probably benign) although imaging cannot exclude malignant foci in such lesions [52, 53].

Limitations of this study were multiple A major limitation was the indistinguishable overlap between premalignant nodules and early hypovascular HCC due to the lack of histopathologic confirmation. The most encountered problematic limitation was the interimage discordance between consecutive dynamic datasets

due to differences in respiratory depths. This was best compensated for using respiratorygated breath-hold expiratory volume acquisitions. User-defined ROIs fail to embody the heterogeneity commonly encountered in tumors. Semiquantitation fails to constitute the signal changes due to disordered arterialization, sinusoidal capillarization, vessel permeability, and interstitial pressure. We tried to offset this using relative metrics such as relative enhancement versus signal intensity and normalized metrics such as r AUC versus AUC.

Conclusions

Multiphase DCE-MRI perfusion analysis is useful as non-invasive tool in many diagnostic dilemmas, the assessment of liver cirrhosis, characterization of cirrhotic nodules, the evaluation of multistep hepatocellular carcinogenesis, and the diagnosis of HCC post-management recurrence.

Abbreviations

DNS	Dysplastic nodules
HCC	Hepatocellular carcinoma
MRI	Magnetic resonance imaging
DCE	Dynamic contrast enhanced
ROI	Region of interest
WIR	Wash-in ratio
WOR	Washout ratio
MRE	Maximal relative enhancement
AUC	Areas under the curve
MTT	Mean transit time

Acknowledgements

Not applicable.

Author contributions

AME collected the data. MAA performed part of the reporting and helped to draft the manuscript. MIY reported the cases. All authors have read and approved the final manuscript.

Funding

This study had no funding from any resource.

Availability of data and materials

The datasets used and/or analyzed during the current study are available from the corresponding author on reasonable request.

Declarations

Ethics approval and consent to participate

Ethics approval and consent to participate Approval for this study was obtained All study procedures were carried out in accordance with the Declaration of Helsinki regarding research involving human subjects. Consent to participate was waived.

Consent for publication

Consent to publish is not applicable.

Competing interests

There are no conflicts of interests. The authors declare that they have no competing interests.

Author details

[1]Department of Radiodiagnosis, Nasser Institute for Research and Treatment, Kornish El Nile, Cairo, Egypt. [2]Present Address: Department of Radio-Diagnosis and Intervention, Faculty of Medicine, University of Alexandria, 10 Shamplion Street, Elazareeta, Alexandria, Egypt. [3]Department of Radiology, Faculty of Medicine, Benha University, Banha, Egypt.

Received: 14 June 2023 Accepted: 17 October 2023
Published online: 24 October 2023

References

1. Gordillo M, Evans T, Gouon-Evans V (2015) Orchestrating liver development. Development 142:2094–2108
2. Mitchell DG, Bruix J, Sherman M et al (2014) LI-RADS (liver imaging reporting and data system): Summary, discussion, consensus of the LI-RADS management working group and future directions. Hepatology 61(3):1056–1065
3. Bosch J, Groszmann RJ, Shah VH (2015) Evolution in the understanding of the pathophysiological basis of portal hypertension: How changes in paradigm are leading to successful new treatments. J Hepatol 62:S121–S130
4. Villanueva A (2019) Hepatocellular carcinoma. N Engl J Med 380:1450–1462
5. Ou HY, Bonekamp S, Bonekamp D et al (2013) MRI arterial enhancement fraction in hepatic fibrosis and cirrhosis. Am J Roentgenol 201:596–602
6. Saito K, Ledsam J, Sourbron S et al (2013) Assessing liver function using dynamic Gd-EOB-DTPA-enhanced MRI with a standard 5-phase imaging protocol. J Magn Reson Imaging 37:1109–1114
7. Chouhan MD, Mark M, Rajeth P et al (2016) Vascular assessment of liver disease—towards a new frontier in MRI'. Br J Radiol 89(1064):20150675
8. Llovet JM, Zucman-Rossi J, Pikarsky E et al (2016) Hepatocellular carcinoma. Nat Rev Dis Prim 2:18
9. Wilson SR, Lyshchik A, Piscaglia F et al (2018) CEUS LI-RADS: algorithm, implementation, and key differences from CT/MRI. Abdom Radiol 43(1):127–142
10. Schram C, Kaufmann S, Rempp H et al (2015) Imaging of HCC-current state of the Art. Diagnostics 5(513–4):5
11. Trabulo D, Santos P, Goncalves A et al (2016) Hepatocellular carcinoma in cirrhotic liver: new perspectives in diagnostic imaging. BJMMR 11:1–14
12. Kobayashi S, Kozaka T, Gabata G et al (2020) Intraarterial and intravenous contrast enhanced CT and MR imaging of multi-step hepatocarcinogenesis defining the early stage of hepatocellular carcinoma development. Hepatoma Research 20:12
13. Liu K, Zhang X, Xu W et al (2017) Targeting the vasculature in hepatocellular carcinoma treatment: starving versus normalizing blood supply. CTG 8:e98–e11
14. Zou J, Balter J, Cao Y (2020) Estimation of pharmacokinetic parameters from DCE-MRI by extracting long and short time-dependent features using an LSTM network. Med Phys 47:3447–3457
15. Zhang W, Chen HJ, Wang ZJ et al (2016) Dynamic contrast enhanced MR imaging for evaluation of angiogenesis of hepato cellular nodules in liver cirrhosis in N-nitrosodiethylamine induced rat model. Eur Radiol 27(5):2086–2094
16. Ueda K et al (2014) Tumor Hemodynamics and Hepatocarcinogenesis: radio pathological correlations and outcomes of carcinogenic hepatocyte nodules. ISRN Hepatol 14:1–11
17. Watanabe A, Ramalho M, Alobaidy M et al (2015) Magnetic resonance imaging of the cirrhotic liver: an update. World J Hepatol 7:468–87
18. Cong B, Wang X, Guo W et al (2023) Prognosis of patients with hepatocellular carcinoma treated with trans arterial chemoembolization (MC-hcc AI 001): development and validation of the ALFP score. J Hepatocell Carcinoma 10:1341–1351
19. Huh J, Kim KW, Kim J et al (2015) Pathology-MRI correlation of hepatocarcinogenesis: recent update. J Pathol Transl Med 49:218–229
20. Choi J-Y, Lee J-M et al (2014) CT and MR imaging diagnosis and staging of hepatocellular carcinoma: Part I. development, growth, and spread: key pathologic and imaging aspects. Radiology 272(3):635–54

21. Cuenod CA, Balvay D (2013) Perfusion and vascular permeability: basic concepts and measurement in DCE-CT and DCE-MRI. Diagn Interv Imaging 94(12):1187–1204
22. Horsman MR, Vaupe IP (2016) Pathophysiological basis for the formation of the tumor microenvironment. Front Oncol 6:16–30
23. Elzeneini A, Yousef M, Refaat M (2018) The role of dynamic contrast-enhanced MRI analysis of perfusion changes in hepatocellular carcinoma'. Benha Med J 35(3):277
24. Chiang J, Sparks H, Rink J et al (2023) Dynamic contrast-enhanced MR imaging evaluation of perfusional changes and ablation zone size after combination embolization and ablation therapy. J Vasc Interv Radiol 34(2):253–260
25. Lin CN, Liao YS, Chen WC et al (2016) Use of myometrium as an internal reference for endometrial and cervical cancer on multiphase contrast-enhanced MRI. PLoS ONE 11:1–12
26. Bin CB, Shih TTF (2014) DCE-MRI in hepatocellular carcinoma-clinical and therapeutic image biomarker. World J Gastroenterol 20:3125–3134
27. Do RKG, Rusinek H, Taouli B (2009) Dynamic contrast-enhanced MR imaging of the liver: current status and future directions. Magn Reson Imaging Clin N Am 17:339–349
28. Filozof CM, Carolen L, Manuel R et al (2022) Best practices in liver biopsy histologic assessment for nonalcoholic steatohepatitis clinical trials: Expert opinion. GastroHep 6:1–11
29. Petitclerc L, Gilbert G, Nagyuen B et al (2017) Liver fibrosis quantification by magnetic resonance imaging. Top Magn Reson Imaging 26(6):229–241
30. Lin S, Hoffmann K, Schemmer P (2012) Treatment of hepatocellular carcinoma: a systematic review. Liver Cancer 1:144–158
31. Ramalho M, Ap M (2017) Magnetic resonance imaging of the cirrhotic liver: diagnosis of hepatocellular carcinoma and evaluation of response to treatment. Radiologia Brasileira Part 2 50:115–125
32. Cho ES, Choi JY (2015) MRI features of hepatocellular carcinoma related to biologic behavior. Korean J Radio 16:449–464
33. Luo L, Yan R (2023) Radiofrequency ablation of hepatocellular carcinomas adjacent to the gallbladder without isolation under contrast-enhanced ultrasound monitoring: a comparative study with long term follow-up. J Hepatocell Carcinoma 10:631–642
34. Shah ZK, McKernan MG, Hahn PF et al (2007) Enhancing and expansile portal vein thrombosis: value in the diagnosis of hepatocellular carcinoma in patients with multiple hepatic lesions. AJR Am J Roentgenol 188:1320–1323
35. Romeo V, Stanzion A, Ugga L et al (2022) Clinical indications and acquisition protocol for the use of dynamic contrast-enhanced MRI in head and neck cancer squamous cell carcinoma: recommendations from an expert panel. Insights Imaging 13(1):17–18
36. Florea A, Mottaghy F, Bauwens M (2021) Molecular imaging of ANGIOGENESIS IN ONCOLOGY: current preclinical and clinical status'. Int J Mol Sci 22(11):5544
37. Pham TT, Wong K, Leni G et al (2022) Dynamic contrast-enhanced magnetic resonance imaging evaluation of whole tumor perfusion heterogeneity predicts distant disease-free survival in locally advanced rectal cancer. Clin Oncol 34(9):561–570
38. Hall TJ, Garra BS, Carson PL et al (2016) A quantitative imaging biomarker alliance. J Acoust Soc Am 140:3188–3189
39. DelliPizzi A, Mastrodicasa D, Cianci R et al (2021) Multimodality imaging of hepatocellular carcinoma: from diagnosis to treatment response assessment in everyday clinical practice. Can Assoc Radiol J 72:714–727
40. Palmisano A, Esposito A, Rancoate P et al (2018) Could perfusion heterogeneity at dynamic contrast-enhanced MRI be used to predict rectal cancer sensitivity to chemoradiotherapy? Clin Radiol 73(10):60
41. Kim SR et al (2008) superiority of CT arterioportal angiography to contrast-enhanced CT and MRI in the diagnosis of hepatocellular carcinoma in nodules smaller than 2CM. J Hepatol 48:382–7
42. Kitao A, Zen Y et al (2009) Hepatocarcinogenesis multistep changes of drainage vessels at CT during arterial portography and hepatic arteriography–radiologic pathologic correlation. Radiology 252:605–614
43. Heimbach JK, Kulik LM, Finn RS et al (2018) AASLD guidelines for the treatment of hepatocellular carcinoma. Hepatology 67(1):358–380
44. Gordon Y, Partovi S, Muller-Eschner M et al (2014) Dynamic contrast -enhanced magnetic resonance imaging: fundamentals and application to the evaluation of the peripheral perfusion. Cardiovasc Diagn Ther 4:147–164
45. O'Connor JPB, Tofts PS, Miles KA et al (2011) Dynamic contrast-enhanced imaging techniques: CT and MRI. Br J Radial 84:8112–8120
46. Wang J, Chen L, Tsang Y et al (2004) Analysis of perfusion changes in advanced hepatocellular carcinoma treated with an antiangiogenic agent: a preliminary study. Am J Roentgenol 183(3):713–719
47. Ippolito D, Colombo M, Trattenero C et al (2015) Diagnostic value of semiquantitative analysis of dynamic susceptibility contrast magnetic resonance imaging with GD-EOB-DTPA in focal liver lesions characterization: a feasibility study. Gastroenterol Res Pract 15:1–7
48. Wang L, Van den Bos IC, Hussain SM et al (2008) Post-processing of dynamic gadolinium-enhanced magnetic resonance imaging exams of the liver: explanation and potential clinical applications for color-coded qualitative and quantitative analysis. Acta Radiol 49:6–18
49. Yamashita Y, Fan ZM, Yamamoto H et al (1994) S and dynamic gadoliniumenhanced FM imaging of hepatocellular carcinoma: correlation with histopathologic findings. JMRI 4:83–90
50. Choi J-Y, Lee J, Sirlin CB (2014) CT and MR imaging diagnosis and staging of hepatocellular carcinoma: part II. Extra cellular agents, hepatobiliary agents, and ancillary imaging features. Radiology 273:30–50. https://doi.org/10.1148/radiol.14132362
51. Elmohr M, Elsayes K, Chernyak V (2021) LI-RADS: review and updates. Clin Liver Dis 17(3):108–112. https://doi.org/10.1002/cld.991-Pubmed
52. Flusberg M, Ganeles J, Ekinci T et al (2017) Impact of a structured report template on the quality of CT and MRI reports for hepatocellular carcinoma diagnosis. J Am Coll Radiol 14(9):1206–1211
53. Taouli B, Johnson RS, Hajdu CH et al (2013) Hepatocellular carcinoma: perfusion quantification with dynamic contrast-enhanced MRI. Am J Roentgenol 201:795–800. https://doi.org/10.2214/AJR.12.9798

Publisher's Note